Polymer light-emitting electrochemical cells: Doping, luminescence, and mobility

Ludvig Edman,[1,*] Melissa A. Summers,[1,2] Steven K. Buratto,[1,2] and Alan J. Heeger[1,3]
[1]*Center for Polymers and Organic Solids, University of California at Santa Barbara, Santa Barbara, California 93103, USA*
[2]*Department of Chemistry and Biochemistry, UCSB, Santa Barbara, California 93106, USA*
[3]*Department of Physics and Materials Department, UCSB, Santa Barbara, California 93106, USA*
(Received 10 February 2004; published 23 September 2004)

We utilize the planar "surface cell" device configuration with Au contacts and a mixture of a soluble phenyl-substituted poly(para-phenylene vinylene) copolymer ("superyellow"), a dicyclohexano-18-crown-6 crown ether, and a $LiCF_3SO_3$ salt as the active material. Because the lowest thermal transition occurs well above room temperature (RT), we can study the charging process at an elevated temperature and probe the exact location of the electroluminescence (EL) and doping-induced quenching of photoluminescence in charged devices at RT. We also employ the same active material in thin-film field-effect transistor structures to study the influence of electrochemical doping on transistor performance. Our results demonstrate that reversible bipolar electrochemical doping indeed takes place at applied voltages above the band gap of the semiconducting polymer ($V \geqslant E_g/e$), but also that limited unipolar electrochemical doping can take place at $V < E_g/e$ if the barrier heights for hole and electron injection are asymmetric. The EL originates in, or in close proximity to, the thin *p-i-n* junction, which is located close to the cathode.

DOI: 10.1103/PhysRevB.70.115212 PACS number(s): 78.55.Kz

I. INTRODUCTION

Polymer light-emitting electrochemical cells (LEC's) represent an interesting alternative to conventional light-emitting diodes (LED's) for use in, e.g., flat-panel display applications. Polymer LEC's can be processed directly from solution and printed onto flexible substrates, thus enabling inexpensive, large-area coverage in many configurations. Moreover, the low turn-on voltage for light output from a polymer LEC, corresponding to the band gap of its constituent semiconducting polymer ($V_{turn\text{-}on} = E_g/e$, where e is the elementary charge), is independent of the thickness of the active layer and the selection of electrode materials.[1,2] This is in sharp contrast to organic (small molecule and polymer) LED's, which require a low-work-function cathode and a high-work-function anode in conjunction with a very thin layer of active material to emit light at a low applied voltage.[3,4]

The fundamental difference between organic LED's and polymer LEC's is that the latter contain mobile ions admixed into the active layer. These ions accumulate close to the electrode interfaces following the application of an external voltage in order to electrically screen the bulk of the material. What happens after the formation of these electric double layers at $V_{turn\text{-}on} \geqslant E_g/e$ has been rationalized by different models.[5–12] However, experimental observations[1,2,9,11,13–17] have demonstrated that the semiconducting polymer becomes electrochemically doped: injected holes attract anions and injected electrons attract cations, establishing *p*-type doping next to the anode and *n*-type doping next to the cathode, respectively, while preserving electroneutrality. With time, these doped regions grow close together, and an *in situ* *p-i-n* junction is formed; *i* represents the relatively thin insulating region, separating the *p*- and *n*-doped regions, over which a large portion of the applied voltage drops under steady-state operation. Subsequently injected holes and electrons migrate through the high-conductivity doped regions before recombining radiatively in or very close to the thin *i* region.[1,2,8]

The mobility of ions is critical during the LEC charging process—i.e., during the initial redistribution of ions and the subsequent electrochemical doping. Ion mobility is, however, not necessary (and is in fact a source of degradation) during steady-state operation after the formation of the *p-i-n* junction. Note that for charging to take place, it is sufficient that one of the ionic species is mobile, as proven by the successful operation of luminescent single-ion conductor LEC's.[18,19] In general, ion mobility is dependent on the redistribution of free volume, which means that the ion mobility approaches zero when the temperature (T) of an LEC is lowered below the glass transition temperature (T_g) and the melting temperature (T_m) of all constituent phases. Consequently, an LEC can be charged at a high T and then operated in the so-called "frozen-junction" mode at a temperature below T_g and T_m of all the constituent phases. Gao *et al.* were the first to make use of this concept, when they charged an LEC (with its lowest thermal transition at $T_g \geqslant 208$ K) at room temperature (RT) and then successfully operated it with fast-response light emission all the way up to $T = 200$ K.[20,21]

For this study, we utilize the planar "surface cell" device configuration with Au contacts and a mixture of a soluble phenyl-substituted poly(para-phenylene vinylene) (PPV) copolymer ("superyellow"), a dicyclohexano-18-crown-6 crown ether, and a $LiCF_3SO_3$ salt as the active material. For this material, the lowest thermal transition occurs well above room temperature, thus conveniently allowing for frozen-junction operation of charged devices at RT.[22,23] We carefully study the charging process of a planar surface cell LEC at an elevated temperature and probe the exact location of the electroluminescence (EL) and doping-induced quenching of photoluminescence (PL) in such charged devices at RT. We also employ the same active material in thin-film field-effect transistor (TFT) structures to study the influence of electro-

chemical doping on transistor performance. Our results demonstrate that reversible bipolar electrochemical doping indeed takes place at applied voltages above the band gap of the semiconducting polymer, but also that limited unipolar electrochemical doping can take place at an applied voltage *below* the band gap. We suggest that the limited unipolar electrochemical doping occurs because the Fermi level of the electrodes (in this case Au) is significantly closer to the valence-band edge than to the conduction-band edge of the luminescent semiconducting polymer. We calculate the doping level as a function of interelectrode distance in such a scenario and find good agreement with the data. We also demonstrate that EL originates in, or in close proximity to, the thin *p-i-n* junction, which is located close to the cathode. The latter indicates that the hole mobility is larger than the electron mobility in superyellow.

II. EXPERIMENT

The electroluminescent polymer, a soluble phenyl-substituted PPV copolymer (superyellow), was synthesized by Covion.[24,25] The crown ether cis-anti-cis-dicyclohexano-18-crown-6 (DCH18C6) was purchased from Acros Organics and dried at 40 °C in a vacuum oven before use. The $LiCF_3SO_3$ salt was purchased from Aldrich and dried at 150 °C for 24 h in a vacuum oven before use. The molecular structures of the three components are presented in the top part of Fig. 1. Two solutions were made by dissolving 5.3 mg superyellow in 1 mL of anhydrous toluene, and 20 mg DCH18C6 and 4.2 mg $LiCF_3SO_3$ in 1 mL of anhydrous toluene, respectively. After prolonged stirring, 135 μL of the superyellow solution was mixed with 50 μL of the DCH18C6-$LiCF_3SO_3$ solution, making the overall (superyellow:DCH18C6:$LiCF_3SO_3$) mass ratio (10:14:3) and the solid-state salt concentration ~1 M. The master solution was stirred on a magnetic hot plate for 24 h at room temperature and 2 h at 60 °C.

For planar surface cells in a top-contact configuration (see middle part of Fig. 1), thin films of the active material were prepared by spin casting (at 1700 rpm for 60 s) the hot master solution onto carefully cleaned glass substrates (sonicated in detergent, rinsed in de-ionized water, sonicated in acetone, sonicated in isopropanol, dried at 120 °C for 12 h). The films were annealed and dried at 75 °C for 3 h. Finally, 100-nm-thick Au electrodes were thermally evaporated at a pressure of $p \sim 10^{-4}$ Pa through a shadow mask establishing the interelectrode distance at $d \approx 40$ μm.

The bottom-contact TFT structure is presented in the bottom part of Fig. 1. TFT structures were prepared by thermally growing a 200-nm-thick SiO_2 dielectric layer onto an *n*-doped Si wafer. For TFT's and planar surface cells in the bottom-contact configuration, Au electrodes (45 nm thickness) on a thin Ti adhesion layer (2 nm thickness) were fabricated by lift-off photolithography. The interelectrode channel length was 5 μm, and the channel width was 1000 μm. Thin films of the active material were deposited onto these structures by drop-casting the hot master solution. After the films appeared dry to the naked eye, the devices were annealed and dried at 75 °C for 3 h. All preparation steps involving the active material took place in an N_2-filled glove box ($O_2 < 1$ ppm).

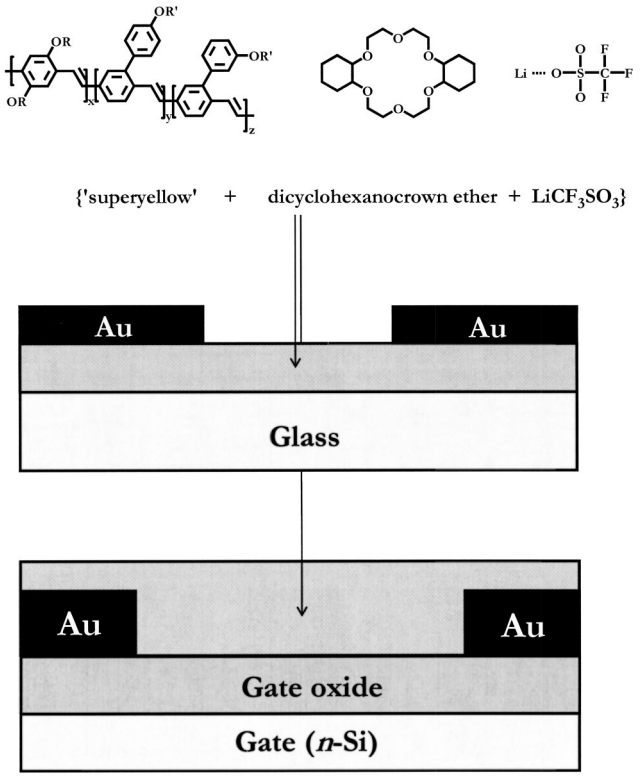

FIG. 1. Molecular structure of the components of the active material (top), schematic device structure of a top-contact planar surface cell (middle), and schematic device structure of a bottom-contact thin-film field-effect transistor (bottom).

Device charging and testing were performed under dynamic vacuum ($p < 10^{-3}$ Pa) with the sample mounted onto the copper block of a cryostat. For planar surface cells, the current was measured via a precision resistor connected to a Keithley 181 nanovoltmeter, and the brightness was measured with a GCA/McPherson photomultiplier module connected to a HP 3478A multimeter. TFT's were characterized using a Keithley 4200 Semiconductor Parameter Analyzer, with the source electrode grounded.

PL and EL intensities as a function of interelectrode position, with a resolution of approximately 300 nm, were established by laser scanning confocal microscopy. The experimental apparatus has been described previously.[26] A custom-built vacuum sample chamber with electrical feedthroughs mounted on a piezoceramic scanning stage was employed. The 457-nm line of an Ar+ laser (Spectra-Physics) was used as the excitation source for PL experiments, with a nominal power density of ~500 mW/cm^2. A laser notch filter (Kaiser Optical) removed scattered laser light, ensuring that only sample PL was transmitted to the avalanche photodiode (APD) detector. For EL imaging, the confocal focus was first established with the laser. Then the laser beam was blocked from the microscope and emission resulting from device operation was focused onto the APD. The PL and EL intensities were obtained by averaging the recorded signal over an area of approximately 40 μm of channel width. Confocal reflec-

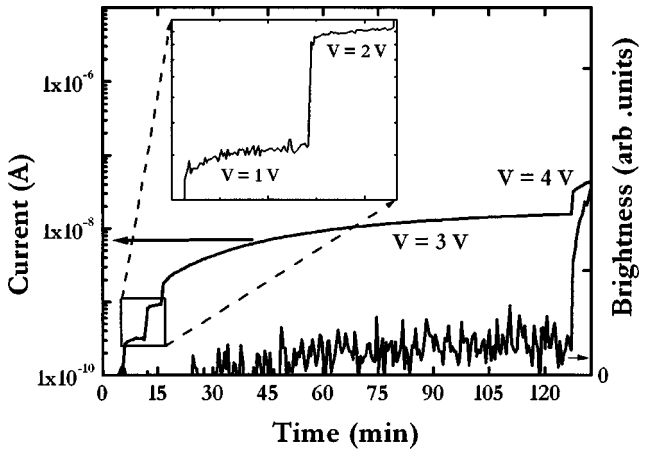

FIG. 2. Current (left) and brightness (right) as a function of time during operation at various applied voltages at $T=85\,^{\circ}\mathrm{C}$ for a bottom-contact Au/{superyellow+DCH18C6+$LiCF_3SO_3$}/Au surface cell with an interelectrode gap of 5 μm. The inset shows a magnification of the current response to $V=1$ V and $V=2$ V.

tion was used to determine the position of the reflective Au electrodes with respect to the observed EL and PL. A low laser power (<1 mW/cm^2) was focused onto the sample, and the laser notch filter was removed. The intensity of reflected laser light incident on the APD was recorded.

III. RESULTS AND DISCUSSION

A. Device charging

Figure 2 presents current and brightness as a function of time at different applied voltages (V) for a bottom-contact Au/{superyellow+DCH18C6+$LiCF_3SO_3$}/Au surface cell operated at $T=85\,^{\circ}\mathrm{C}$. In a previous publication, we demonstrated that such a device only can be charged at an elevated temperature and that frozen-junction operation is possible at RT.[22] We rationalized this behavior by showing that the active material phase-separates into a superyellow phase with a glass transition at $T_g \approx 180\,^{\circ}\mathrm{C}$ and a crystalline DCH18C6-$LiCF_3SO_3$ phase which melts at $T_m \approx 56\,^{\circ}\mathrm{C}$, consequently only allowing for ion mobility and charging at $T \geqslant 56\,^{\circ}\mathrm{C}$.[22] Figure 2 includes data obtained at applied voltages that are both below and above the optical band gap of the superyellow polymer ($E_g=2.4$ eV).[27] For $V<E_g/e$ (see the magnified portion in the inset in Fig. 2), the trend is that the current at a set V initially increases with time but after some time levels out at a limiting value. The time constant is dependent on the interelectrode distance and the bias history of the sample, but the same general behavior is observed also for thicker cells. For $V=3$ V ($>E_g/e$), the trend is that the current increase, and thus charging, continues for significantly longer times. Light emission (the signature of bipolar injection) of a weak magnitude is detected after $\sim$10 min at $V=3$ V, while light visible to the naked eye is observed after prolonged charging at $V=6$ V (not shown).

The charging of a polymer LEC is typically described as a two step-process: (i) an initial electric double-layer formation at the interfaces to electrically screen the bulk of the polymer and (ii) a subsequent simultaneous electrochemical p- and n-type doping of the semiconducting polymer if $V \geqslant E_g/e$. The time required for the formation of the electric double layers (t_{DL}) should be approximately related to the RC-charging time of a symmetric electrochemical capacitor (t_{RC}):

$$t_{DL} \approx t_{RC} = (L/\sigma A)(A\varepsilon_0\varepsilon_r/2L_{DL}), \tag{1}$$

where L ($=5\times10^{-6}$ m) is the interelectrode distance, σ is the ionic conductivity of the active material, A is the electrode/active material interfacial area, ε_0 ($=8.854\times10^{-12}$ C^2/Nm^2) is the permittivity of free space, ε_r is the effective dielectric constant within the electric double layers, and L_{DL} is the thickness of the electric double layers. Using values of $\sigma=10^{-4}$ S/m,[2] $\varepsilon_r=6$,[16] and $L_{DL}=1\times10^{-9}$ m,[28] we obtain a very short t_{DL} of $\approx$1.4 ms.

Ouisse and co-workers[29] and de Mello and co-workers[7] found t_{DL} of the order of seconds in certain thin "sandwich cell" LEC's, but the former authors demonstrated that such slow kinetics are due to rough interfaces, originating in thermal evaporation of top electrodes on a soft active material and/or significant phase separation. The LEC device presented in Fig. 2 contains an active material with a minimal phase separation on a $\sim$25-nm scale (see Ref. 22), which was deposited on top of photolithographically prepatterned electrodes, and thus a long t_{DL} is unlikely. Furthermore, the current is expected to decay with time during electric double-layer formation (as was also the case for the slow devices of Ouisse *et al.* and de Mello *et al.*),[29,7] which is in conflict with the observed increase in current with time in Fig. 2. Consequently, as discussed in detail below, limited electrochemical doping of the semiconducting polymer, with a concomitant increase in conductivity and current, appears to take place for $V<E_g/e$.

B. Luminescence and junction properties

It is well established that PL is quenched by low levels of doping via exciton diffusion to nearby hole or electron quenching sites.[30,31] Estimates of the range of exciton diffusion in PPV-based polymers range from 8 to 13 nm.[32,33] Thus, PL quenching will be significant at doping levels of $\sim10^{17}$ cm^{-3} but also detectable even at $\sim10^{16}$ cm^{-3}. Figure 3 presents the PL intensity as a function of distance from anode (left) to cathode (right) at RT for a frozen-junction top-contact Au/{superyellow+DCH18C6+$LiCF_3SO_3$}/Au surface cell at open-circuit conditions. The device was charged at $T=85\,^{\circ}\mathrm{C}$ at different voltages and times, $V=2$ V and $t\sim15$ min (dashed line), $V=3$ V and $t\sim15$ min (dotted line), and $V=3$ V and $t\sim30$ min (dash-dotted line); and thereafter cooled to RT under applied voltage. Preceding each new charging, the device was completely discharged under short-circuit conditions at $T=85\,^{\circ}\mathrm{C}$, as demonstrated by a comparison of the PL profile of a discharged device with that of a pristine device. As a reference, the PL intensity for an uncharged device is also included (solid line).

The observation of PL quenching in Fig. 3 demonstrates that electrochemical doping takes place at $T=85\,^{\circ}\mathrm{C}$ and that this doping is "frozen-in" at RT. A small but clearly distin-

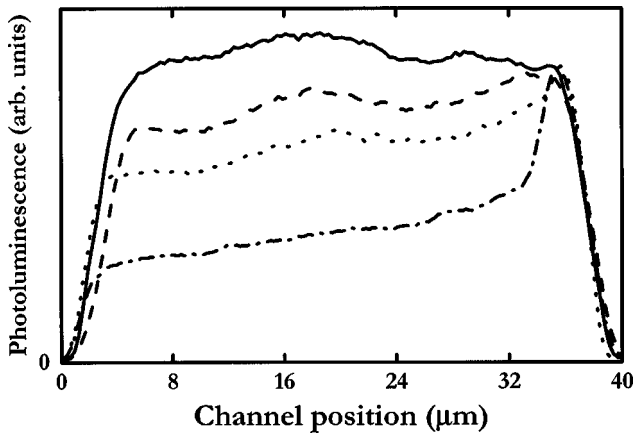

FIG. 3. Photoluminescence intensity as a function of distance from anode (left) to cathode (right) for a top-contact Au/{superyellow+DCH18C6+$LiCF_3SO_3$}/Au surface cell with an interelectrode gap of ~40 μm. The data were collected at RT following high-temperature charging (T=85 °C) at V=2 V for t ~15 min (dashed line), V=3 V and t~15 min (dotted line), and V=3 V and t~30 min (dash-dotted line). The solid line represents data collected from an initially charged device which was completely discharged under short-circuit conditions at T=85 °C.

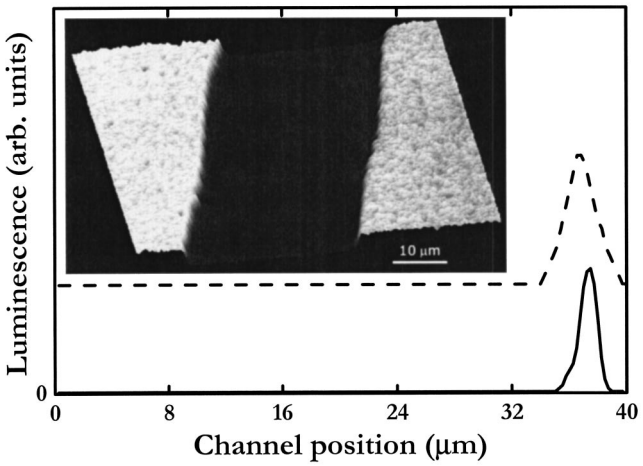

FIG. 4. Electroluminescence (dashed line, up-shifted for clarity) and photoluminescence (solid line) intensity as a function of distance from anode (left) to cathode (right) for a top-contact Au/{superyellow+DCH18C6+$LiCF_3SO_3$}/Au surface cell with an interelectrode gap of ~40 μm. The data were collected at RT following high-temperature charging (T=85 °C) at V=20 V. The inset shows a laser reflection image of the device structure.

guishable amount of doping is apparent following the high-T application of a voltage *below* the band gap—i.e., at V =2 V (compare the dashed line with the solid line)—demonstrating that charging at V=2 V can produce doping levels of ~10^{16} cm^{-3} (see discussion in previous paragraph). For V=3 V ($>E_g/e$) at T=85 °C, the doping-induced PL quenching increases with time (compare the dash-dotted line with the dotted line), although a relatively thin area, located close to the negative cathode (to the right in Fig. 3), remains undoped.

Figure 4 presents EL (dashed line) and PL (solid line) intensities as a function of distance from anode (left) to cathode (right) at RT for an identical frozen-junction top-contact Au/{superyellow+DCH18C6+$LiCF_3SO_3$}/Au surface cell, which was charged at V=20 V and T=85 °C before being cooled to RT under applied voltage. Included as the inset in Fig. 4 is a three-dimensional confocal laser reflection image of the same device, where the Au electrodes appear higher due to their higher reflectivity. The EL from the frozen-junction device originates in a relatively thin zone located close to the cathode (to the right in Fig. 4). The nonquenched PL originates from the same area (the undoped polymer region), although the width of this region appears to be slightly narrower than the width of the EL. The width of the undoped polymer region is approximately 4 μm, corresponding to ≈10% of the interelectrode distance. The undoped region in the more heavily doped device in Fig. 4 approximately coincides with the position of the undoped region in the lightly doped device in Fig. 3, implying that the position and width of the *p-i-n* junction are essentially independent of the magnitude of the charging voltage.

Manzanares *et al.* developed a theoretical model which demonstrates that an emission zone and *p-i-n* junction located close to the cathode are a consequence of the hole mobility being larger than the electron mobility.[8] In this context, it is interesting to note that Martens *et al.* employed admittance spectroscopy to demonstrate that an OC_1C_{10}-PPV polymer (with a molecular structure which is reminiscent of superyellow) exhibits a significantly higher hole mobility than electron mobility.[34] We also note that EL originating from a thin zone close to the cathode has also been observed from LEC's containing (i) a poly(thiophene) with oligo(ethylene oxide) side chains mixed with $LiCF_3SO_3$,[35] (ii) a PPV with alkoxy side chains mixed with poly(ethylene oxide) and $LiCF_3SO_3$,[17] and (iii) a flourene-phenylene vinylene copolymer with aliphatic side chains mixed with poly(ethylene oxide) and $LiCF_3SO_3$.[17] In contrast, PPV without side chains mixed with poly(ethylene oxide) and $LiCF_3SO_3$ exhibits an emission zone close to the center of the device.[1,2,13] The above trend suggests that the addition of certain side chains, aside from inducing solubility, establishes a mobility anisotropy with the hole being the more mobile carrier.

C. Transistor performance

Figure 5 presents the source-drain current (I_{SD}) as a function of source-gate voltage (V_G)—i.e., the transfer characteristics—at RT and a source-drain voltage (V_{SD}) of −10 V for the {superyellow+DCH18C6+$LiCF_3SO_3$} active material in a TFT configuration (see bottom part of Fig. 1 for schematic device structure). The TFT devices were charged at V_{SD}=−2 V and t~30 min (solid line) and V_{SD}=−3 V and t~15 min (dashed line), respectively, before being cooled from T=85 °C to RT under applied voltage. Also, an initially charged TFT was discharged under short-circuit conditions at T=85 °C before being operated at RT (dotted line). The discharged device performs as a pristine device, demonstrating that the electrochemical processes are reversible at T

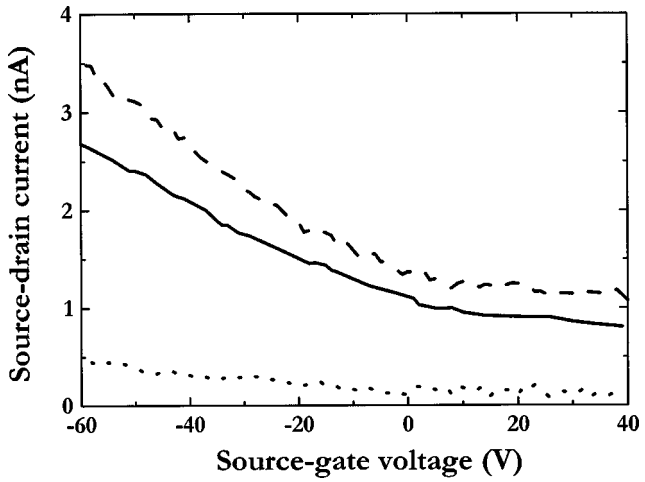

FIG. 5. Source-drain current as a function of source-gate voltage at $V_{SD}=-10$ V and RT for a TFT with {superyellow+DCH18C6 $+LiCF_3SO_3$} as the active material and Au electrodes. The TFT's were charged at $T=85$ °C and $V_{SD}=-2$ V for $t\sim 30$ min (solid line) and $V_{SD}=-3$ V at for $t\sim 15$ min (dashed line), respectively, before being cooled to RT under applied bias. Also, an initially charged TFT was completely discharged at short-circuit conditions at $T=85$ °C and then operated at $V_{SD}=-10$ V and RT (dotted line).

$=85$ °C and that no significant chemical side reactions have taken place.

We have previously reported that this type of ion-containing TFT can be tuned, via a short charging at, e.g., $V_{SD}=-2$ V and $T=85$ °C, to exhibit markedly improved *p*-channel characteristics at RT in the form of an improved on/off ratio and an increased on-current.[36] We demonstrated that the improved device performance was due to the stabilization of ionic layers close to the electrode interfaces, which decreases the injection-barrier widths and establishes a low-resistivity Ohmic contact for hole injection into the polymer.[36] In contrast, electrochemical doping of the bulk will, in addition to improve the injection, create a low-resistivity path in the bulk in parallel to the gate-active part of the polymer. This increases I_{SD} in both the on and off states, but decreases the on/off ratio, and it is consequently not an attractive feature for TFT applications.

The long charging times of the TFT's in Fig. 5 at voltages below and above the band gap of the superyellow polymer—i.e., $V_{SD}=-2$ V (solid line) and $V_{SD}=-3$ V (dashed line), respectively—produce qualitatively identical devices, with both the on- and off-current being significantly higher than in an uncharged TFT (dotted line). This is additional evidence that long-time charging at $V<E_g/e$ produces the same qualitative effect as a long-time charging at a voltage above the band gap—namely, electrochemical doping. In Sec. III D below, we present a model that rationalizes limited unipolar doping after long-time charging at an applied voltage below the band gap for LEC's with asymmetric injection-barrier heights.

D. Model rationalizing limited unipolar electrochemical doping at $V<E_g/e$

de Mello and co-workers[7] and Buda and co-workers[37] have studied polymer LEC's and organic small-molecule

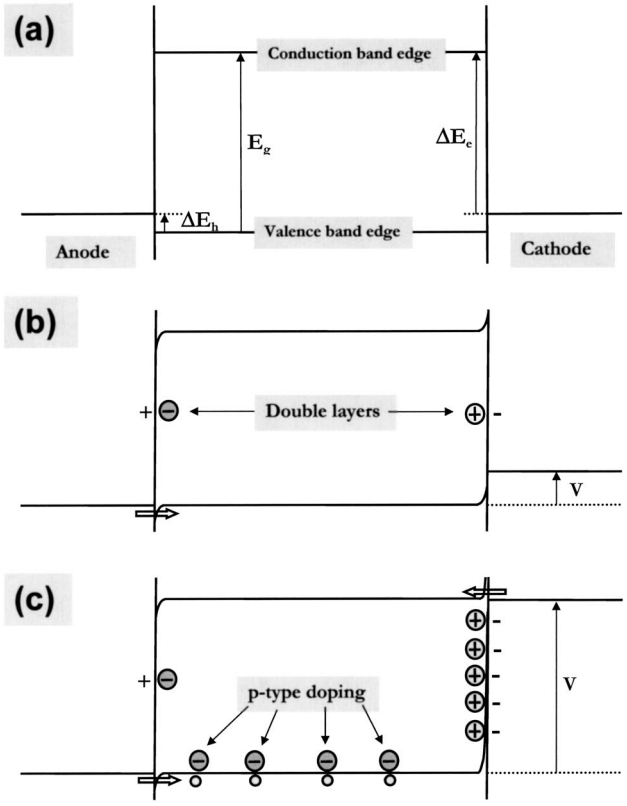

FIG. 6. Schematic electron energy level diagrams for an LEC, containing a semiconducting polymer with a band gap E_g, and with asymmetric barrier heights for hole injection (ΔE_h) and electron injection (ΔE_e). The large circles represent ions, the small open circles represent anion-compensated holes in the bulk (i.e., *p*-type doping), and the arrows represent significant (nonthermally assisted) injection at an interface. The ionic and electronic response to $V=0$ V (a), $V=2\Delta E_h/e$ (b), and $V=E_g/e$ (c) are presented. The asymmetry in the injection barrier heights allows for the onset of tunneling injection of holes and subsequent *p*-type doping at $V=2\Delta E_h/e<E_g/e$.

LEC's, respectively, and have shown that a mismatch in barrier heights at the two electrode/active-material interfaces allow for unipolar injection for a limited V range at $V<E_g/e$. As presented below, a model based on semiconductor terminology demonstrates that limited unipolar electrochemical doping of an ion-containing semiconducting polymer at a voltage below its band gap is possible if the barriers for electron and hole injection are of different heights.

Figures 6(a)–6(c) present electron energy level diagrams at different applied voltages for an LEC, with the height of the hole injection barrier (ΔE_h) significantly lower than the height of the electron injection barrier (ΔE_e). We assume that the electric double layers are sufficiently thin (~ 1 nm) to make hole (electron) injection highly efficient when the Fermi level of the anode (cathode) is aligned with the valence-band edge (conduction-band edge) in the bulk. This is a reasonable assumption for our devices considering the high initial salt concentration (~ 1 M) and that light emission (a signature of bipolar injection) is detected at $V=3$ V (see

Fig. 2). Furthermore, we assume that the electric double-layer formation at the two interfaces is symmetric and consequently that the initial applied voltage is equally distributed between the two electrode/polymer interfaces. Also, no built-in voltage is apparent at $V=0$ V in Fig. 6(a), since LEC devices with identical electrodes were employed. Note, however, that the main results of the model—i.e., Eqs. (3)–(5)—are valid also for the more general case of an LEC with different electrode materials.

Figure 6(b) represents the device at $V=2\Delta E_h/e$. Ionic layers have formed close to the electrodes to electrically screen the bulk of the polymer, so that the applied voltage is dropped only at the two interfaces, half at the anode/polymer interface and half at the polymer/cathode interface. Consequently, at $V=2\Delta E_h/e$ the Fermi level of the anode is aligned with the valence-band edge in the bulk, and with the double layers being very thin efficient tunneling injection of holes is possible. In contrast, the Fermi level of the cathode is still positioned below the conduction-band edge, making significant (nonthermally assisted) electron injection impossible.

When the applied voltage is increased further, the Fermi level of the anode is effectively pinned to the valence-band edge, so that the excess applied voltage is dropped solely at the polymer/cathode interface. This process will continue until the Fermi level of the cathode is aligned with the conduction band edge in the bulk at $V=E_g/e$ [see Fig. 6(c)]. At this point, $\Delta E_h/e$ of the applied voltage is dropped at the anode/polymer interface and $\Delta E_e/e$ is dropped at the polymer/cathode interface to compensate for ΔE_h and ΔE_e, respectively. A direct consequence of the injection-barrier asymmetry is that the number of cations "locked up" in the cathodic double layer exceeds the number of anions in the anodic double layer. To preserve electroneutrality in the bulk, some of the injected holes will compensate the excess of anions to establish limited *p*-type electrochemical doping in the bulk, as schematically pictured in Fig. 6(c).

The electric double layer at an interface is analogous to a parallel-plate capacitor, and thus the net ionic surface charge density in the double layer (Q_{DL}) can be obtained from the following equation:

$$Q_{DL} = V_{DL}\varepsilon_0\varepsilon_r/L_{DL}, \tag{2}$$

where V_{DL} is the voltage drop over the double layer, ε_0 is the permittivity of free space, ε_r is the dielectric constant within the electric double layer, and L_{DL} is its thickness. The net excess ionic surface charge density (Q_{excess}) in the two double layers is equal to

$$Q_{excess} = Q_{DL}(\text{cathode}) - Q_{DL}(\text{anode}). \tag{3}$$

If we simplify somewhat and assume that the compensating ions in the bulk (and consequently the doping) are homogenously distributed over the interelectrode distance (L), the amount of doping due to the injection-barrier-height asymmetry (c') is given by

$$c' = Q_{excess}/eL = \varepsilon_0\varepsilon_r[V_{DL}(\text{cathode}) - V_{DL}(\text{anode})]/eL_{DL}L, \tag{4}$$

where e is the elementary charge. A positive c' value corresponds to *p*-type doping while a negative c' corresponds to *n*-type doping. At $V=E_g/e$ a maximum net doping level (c'_{max}) is attained which is equal to

$$c'_{max} = \varepsilon_0\varepsilon_r(\Delta E_e - \Delta E_h)/e^2L_{DL}L. \tag{5}$$

Equations (3)–(5) are valid also for the more general case of dissimilar cathode and anode materials. Note, however, that an onset of unipolar hole injection at $V=2\Delta E_h/e$ as in Fig. 6(b) (or unipolar electron injection at $V=2\Delta E_e/e$ if $\Delta E_e<\Delta E_h$) is strictly true only for devices with identical cathodes and anodes.

E. Comparison of experimental results with the model

For Au/{superyellow+DCH18C6+$LiCF_3SO_3$}/Au devices, the injection barrier height for holes is expected to be approximately $\Delta E_h=0.5$ eV,[38] and consequently $\Delta E_e=1.9$ eV. If we use values related to our specific devices at $V=2$ V [i.e. $\varepsilon_r=6$,[16] $L_{DL}=1\times10^{-9}$ m,[28] V_{DL} (cathode) $=1.5$ V and V_{DL} (anode) $=0.5$ V] in Eq. (4), we obtain a *p*-type doping level of 7×10^{16} cm^{-3} for a 5-μm-thick device and 8×10^{15} cm^{-3} for a 40-μm-thick device, respectively. Although these values are small, they are sufficient to rationalize the observed experimental results at $V<E_g/e$.

Figure 2 presents current versus time for different V for a 5-μm-thick surface cell at $T=85$ °C. The current initially increases with time following a voltage step, but after a number of minutes levels out at a constant value if $V<E_g/e$. This is consistent with the slow formation of limited *p*-type doping in the bulk, and even though the calculated doping level is modest (7×10^{16} cm^{-3} at $V=2$ V), the combination of a low intrinsic conductivity of superyellow and an Ohmic contact for hole injection (at $V\geqslant1$ V) makes it reasonable that such a doping level will cause an increase in the current. Figure 3 presents the PL quenching of a 40-μm-thick surface cell at RT following charging at $V=2$ V and $T=85$ °C. In Sec. III B, the observed decrease in PL was demonstrated to be correlated to doping on a 10^{16}-cm^{-3} level, a value in good agreement with the calculated doping level of 8×10^{15} cm^{-3}. Finally, Fig. 5 presents the transistor performance at RT for an uncharged TFT and a TFT which had been charged at $T=85$ °C at $V_{SD}=-2$ V for $t\sim30$ min, respectively. The charged device exhibits a significantly higher I_{SD}, in both the on and off states, than the uncharged device. This shows that the conductivity of the active material has increased and consequently that bulk doping has taken place, following a long-time charging at $V_{SD}=-2$ V.

IV. CONCLUSIONS

We have studied the charging process of an Au/{superyellow+DCH18C6+$LiCF_3SO_3$}/Au surface cell at $T=85$ °C and probed the spatial distribution of the PL and

EL intensities of such charged devices at RT. We also employed the same active material in TFT structures and established the transistor performance as a function of charging. Our results show that for $V > E_g/e$, where E_g is the band gap of superyellow, a *p-i-n* junction is formed near the cathode with a thickness of ≈10% of the interelectrode gap. This junction remains even at relatively high doping levels in the nearby *p*-type and *n*-type regions. For $V = 2$ V—i.e., for $V < E_g/e$—we find unambiguous evidence for limited electrochemical doping. We present a model which shows that limited unipolar doping at an applied voltage below the band gap is a direct consequence of an asymmetry in the injection-barrier heights for holes and electrons. The doping levels calculated with this model correlate well with acquired experimental data. Finally, we present indications for that the hole mobility is larger than the electron mobility in superyellow.

ACKNOWLEDGMENTS

The authors are grateful to Dr. Martin Vehse at UCSB, Dr. Klaus Bechgaard at UCSB, Dr. Allen J. Bard at University of Texas at Austin, and Dr. Darryl Smith at Los Alamos National Laboratory for stimulating discussions, and to Dr. Marc Pauchard at UCSB and James Swensen at UCSB for invaluable help with experimental preparations. Research at UCSB was supported by the STC Program of the National Science Foundation under Agreement No. DMR-0120967. L. E. acknowledges generous personal support from the Wenner-Gren foundations and a research grant from Magn. Bergvalls stiftelse.

*Corresponding author. Permanent address: Department of Physics, Umeå University, SE-901 87 Umeå, Sweden. Electronic address: ludvig.edman@physics.umu.se

[1] Q. Pei, G. Yu, C. Zhang, Y. Yang, and A. J. Heeger, Science **269**, 1086 (1995).
[2] Q. Pei, Y. Yang, G. Yu, C. Zhang, and A. J. Heeger, J. Am. Chem. Soc. **118**, 3922 (1996).
[3] C. W. Tang and S. A. Van Slyke, Appl. Phys. Lett. **51**, 913 (1987).
[4] I. D. Parker, J. Appl. Phys. **75**, 1656 (1994).
[5] D. L. Smith, J. Appl. Phys. **81**, 2869 (1997).
[6] I. Riess and D. Cahen, J. Appl. Phys. **82**, 3147 (1997).
[7] J. C. de Mello, N. Tessler, S. C. Graham, and R. H. Friend, Phys. Rev. B **57**, 12 951 (1998).
[8] J. A. Manzanares, H. Reiss, and A. J. Heeger, J. Phys. Chem. B **102**, 4327 (1998).
[9] J. Gao, A. J. Heeger, I. H. Campbell, and D. L. Smith, Phys. Rev. B **59**, R2482 (1999).
[10] J. C. de Mello, J. J. M. Halls, S. C. Graham, N. Tessler, and R. H. Friend, Phys. Rev. Lett. **85**, 421 (2000).
[11] M. Sampietro, R. Sotgiu, F. P. Wenzl, L. Holzer, S. Tasch, and G. Leising, Phys. Rev. B **61**, 266 (2000).
[12] J. C. de Mello, Phys. Rev. B **66**, 235210 (2002).
[13] D. Dick, A. J. Heeger, Y. Yang, and Q. Pei, Adv. Mater. (Weinheim, Ger.) **8**, 985 (1996).
[14] Y. Yang and Q. Pei, Appl. Phys. Lett. **68**, 2708 (1996).
[15] J. Gao, G. Yu, and A. J. Heeger, Adv. Mater. (Weinheim, Ger.) **10**, 692 (1998).
[16] I. H. Campbell, D. L. Smith, C. J. Neef, and J. P. Ferraris, Appl. Phys. Lett. **72**, 2565 (1998).
[17] J. Gao and J. Dane, Appl. Phys. Lett. **83**, 3027 (2003).
[18] V. Cimrová, W. Schmidt, R. Rulkens, M. Schulze, W. Meyer, and D. Neher, Adv. Mater. (Weinheim, Ger.) **8**, 585 (1996).
[19] L. Edman, M. Pauchard, B. Liu, G. Bazan, D. Moses, and A. J. Heeger, Appl. Phys. Lett. **82**, 3961 (2003).
[20] J. Gao, G. Yu, and A. J. Heeger, Appl. Phys. Lett. **71**, 1293 (1997).
[21] J. Gao, Y. Li, G. Yu, and A. J. Heeger, J. Appl. Phys. **86**, 4594 (1999).
[22] L. Edman, M. Pauchard, D. Moses, and A. J. Heeger, J. Appl. Phys. **95**, 4357 (2004).
[23] G. Yu, Y. Cao, M. Andersson, J. Gao, and A. J. Heeger, Adv. Mater. (Weinheim, Ger.) **10**, 385 (1998).
[24] H. Becker, H. Spreitzer, W. Kreuder, E. Kluge, H. Schenk, I. Parker, and Y. Cao, Adv. Mater. (Weinheim, Ger.) **12**, 42 (2000).
[25] H. Becker, O. Gelsen, E. Kluge, W. Kreuder, H. Schenk, and H. Spreitzer, Synth. Met. **111-112**, 145 (2000).
[26] K. D. Weston, P. J. Carson, H. Metiu, and S. K. Buratto, J. Chem. Phys. **109**, 7474 (1998).
[27] L. Edman, D. Moses, and A. J. Heeger, Synth. Met. **138**, 441 (2003).
[28] J. O'M. Bockris, A. K. N. Reddy, and M. Gamboa-Aldeco, *Fundamentals of Electrodics, Modern Electrochemistry*, Vol. 2A (Kluwer Academic, New York, 2000), pp. 871–1036.
[29] T. Ouisse, O. Stéphan, M. Armand, and J. C. Leprêtre, J. Appl. Phys. **92**, 2795 (2002).
[30] S. Hayashi, K. Kaneto, and Y. Yoshino, Solid State Commun. **61**, 249 (1987).
[31] P. Dyreklev, O. Inganäs, J. Paloheimo, and H. Stubb, J. Appl. Phys. **71**, 2816 (1992).
[32] J . J. M. Halls, K. Pichler, R. H. Friend, S. C. Moratti, and A. B. Holmes, Synth. Met. **77**, 277 (1996).
[33] P. J. Hamer, K. Pichler, M. G. Harrison, R. H. Friend, B. Ratier, A. Moliton, S. C. Moratti, and A. B. Holmes, Philos. Mag. B **73**, 367 (1996).
[34] H. C. F. Martens, J. N. Huiberts, and P. W. M. Blom, Appl. Phys. Lett. **77**, 1852 (2000).
[35] Y. Kaminorz, E. Smela, T. Johansson, L. Brehmer, M. R. Andersson, and O. Inganäs, Synth. Met. **113**, 103 (2000).
[36] L. Edman, J. Swensen, D. Moses, and A. J. Heeger, Appl. Phys. Lett. **84**, 3744 (2004).
[37] M. Buda, G. Kalyuzhny, and A. J. Bard, J. Am. Chem. Soc. **124**, 6090 (2002).
[38] R. A. Street and A. Salleo, Appl. Phys. Lett. **81**, 2887 (2002).